Aggregation of Charge Acceptors on Nanocrystal Surfaces Alters Rates of Photoinduced Electron Transfer

Danielle M. Cadena,[1,2] Jakub K. Sowa,[2,3] Daniel E. Cotton,[1] Christopher D. Wight,[1] Cole L. Hoffman,[1] Holden R. Wagner,[1] Jessica T. Boette,[1] Emily K. Raulerson,[1] Brent L. Iverson,[1] Peter J. Rossky,[2,3*] & Sean T. Roberts[1,2*]

[1]*Department of Chemistry, The University of Texas at Austin, Austin, TX 78712, USA*
[2]*Center for Adapting Flaws into Features, Rice University, Houston, TX 77251, USA*
[3]*Department of Chemistry, Rice University, Houston, TX 77251, USA*

[*]Authors to whom correspondence should be sent: roberts@cm.utexas.edu & peter.rossky@rice.edu

Abstract:

Semiconductor nanocrystals (NCs) interfaced with molecular ligands that function as charge and energy acceptors are an emerging platform for the design of light harvesting, photon upconverting, and photocatalytic materials. However, several NC systems explored for these applications often feature high concentrations of bound acceptor ligands, which can lead to ligand-ligand interactions that may alter each system's ability to undergo charge and energy transfer. Here, we demonstrate that aggregation of acceptor ligands impacts the rate of photoinduced NC-to-ligand charge transfer between lead (II) sulfide (PbS) NCs and perylenediimide (PDI) electron acceptors. As the concentration of PDI acceptors is increased, we find the average electron transfer rate from PbS to PDI ligands decreases by nearly an order of magnitude. The electron transfer rate slowdown with increasing PDI concentration correlates strongly with the appearance of PDI aggregates in steady-state absorption spectra. Electronic structure calculations and molecular dynamics simulations suggest that PDI aggregation slows the rate of electron transfer by reducing orbital overlap between PbS charge donors and PDI charge acceptors. While we find aggregation slows electron transfer in this system, the computational models we employ predict that ligand aggregation could also be used to speed electron transfer by producing delocalized states that exhibit improved NC-molecule electronic coupling and energy alignment with NC conduction band states. Our results demonstrate that ligand aggregation can alter rates of photoinduced electron transfer between NCs and organic acceptor ligands and should be considered when designing hybrid NC:molecule systems for charge separation.

Introduction

Hybrid materials that interface semiconductor nanocrystals (NCs) with molecular chromophores have attracted great interest as they can harness the complementary properties of these materials to facilitate photodriven charge separation and spin-selective energy transfer.[1–7] The high extinction coefficients and size-dependent optoelectronic properties of NCs make them well suited to serve as light harvesters,[8–10] while their tunable surface chemistries and large surface areas allows them to simultaneously bind redox-active molecular charge acceptors.[11] Photoexcitation of these materials can drive charges from a NC to a molecular acceptor, which has been used to generate solar fuels and other redox products.[12,13]

Photoexciting a NC can also generate excitons with mixed spin character as NCs generally possess small exchange splitting between their spin states as well as strong spin-orbit coupling due to their inclusion of heavy atoms.[8,14] In hybrid NC:molecule systems, this permits a NC to populate dark triplet exciton states on molecular acceptors via triplet energy transfer.[15,16] This process has recently been used to great effect to catalyze stereoselective synthesis of biomolecules.[5,17] Moreover, NC-to-molecule triplet energy transfer can also be used to fuel triplet fusion, a process wherein pairs of molecules placed in a triplet excited state share their energy to place one molecule in the pair in an emissive, high-energy spin-singlet state.[18–20] Triplet fusion fueled by NC:molecule hybrids has readily been used to upconvert red and near-infrared light into the visible spectral range,[2,3,14,15,21] which can be used to improve solar energy capture[22,23] and generate high-energy photons for 3D printing.[24]

Each of these applications require either charge carriers or excitons with distinct spin multiplicity to be transferred across the NC:molecule interface efficiently. Both electron transfer and triplet exciton transfer are mediated by the direct exchange of electrons, which requires spatial

overlap of the participating donor and acceptor orbitals.[14,25–31] To enhance this overlap, molecular acceptors are often bound to NC surfaces as ligands via short chemical tethers. Preparation of NC:molecule systems often entails maximizing the surface concentration of molecular acceptors during ligand exchange as the rate of NC-to-molecule transfer is expected to increase linearly with acceptor concentration according to:[32–35]

$$k_{ET} = N_{Acceptor} k_{ET}^{0} \quad (1)$$

Here, k_{ET} is the electron transfer rate for a photoexcited NC that binds $N_{Acceptor}$ molecular acceptors and k_{ET}^{0} is the average rate of transfer per acceptor (i.e. the intrinsic transfer rate). For low concentrations of acceptors, NC:molecule systems obey Eq. 1 well. For example, the rate of charge transfer from cadmium sulfide NCs to methyl viologen electron acceptors was found to increase linearly with acceptor surface concentration.[32]

However, as the acceptor surface concentration increases, strong deviations from Eq. 1 can be observed. For example, several NC-based photon upconversion systems wherein NC-to-molecule triplet energy transfer plays a major role were found to exhibit upconversion quantum yields that initially increased with increasing acceptor surface concentration, in agreement with Eq. (1), before undergoing a precipitous drop with further increases in acceptor concentration.[22,36] The authors of these studies speculated that the reduction in upconversion quantum yield at high ligand loadings was the result of acceptor ligand aggregation, but gave no physical mechanism linking aggregation to reduced energy transfer rates.

Introducing a high concentration of acceptor ligands to a NC surface has the potential to promote ligand-ligand interactions that can influence key structural and energetic parameters that control charge migration across NC:molecule interfaces. **Figure 1** describes how aggregation-induced perturbations to the physical structure of a NC's ligand shell and the electronic structure

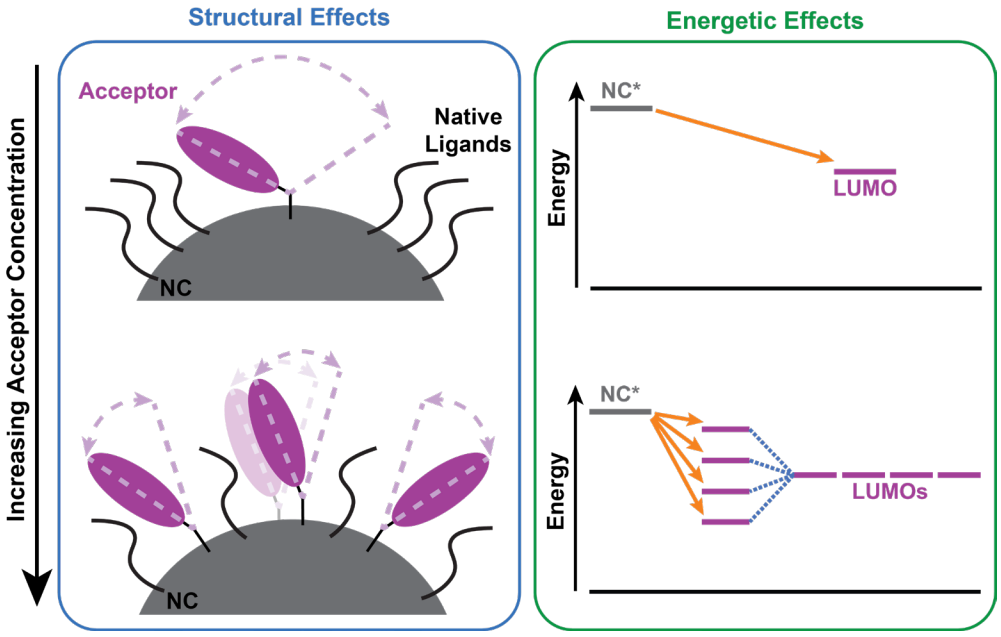

Figure 1: Mechanisms by which the aggregation of charge acceptors on NC surfaces can impact photoinduced charge transfer. (Left) Aggregation can alter the orientational space that can be explored by acceptors, thereby altering their ability to accept charge by approaching the NC surface. (Right) Aggregation can split the energy levels of charge acceptors into a band of states that each have a different energetic driving force and electronic coupling for charge transfer.

of molecular acceptors can each act to modify NC-to-acceptor charge transfer rates. At low acceptor concentrations, single acceptor ligands are free to explore many orientational conformations among a ligand shell comprised of mostly flexible native ligands, such as oleate (**Figure 1**, left). With the addition of more acceptors, attractive interactions between surface-bound acceptors can limit their range of motion and ability to approach the NC surface, thereby reducing the electronic coupling between the NC and bound acceptors.

Likewise, at high concentrations acceptor aggregation can also impact the electronic states that act to receive charge from a NC. Following Marcus Theory,[37] the rate of NC-to-molecule charge transfer is dependent on the redox energy level alignment between the NC donor and molecular acceptor as the energetic offset between these excited states will define the free energy change for charge transfer. In the case of an acceptor monomer, energy transfer occurs from an excited state on a NC to one localized on a single acceptor (**Figure 1**, right). However, molecular

aggregation can cause the orbitals of neighboring acceptors to couple to one another, producing new electronic states whose energy splitting reflects the strength of the inter-acceptor coupling.[38] The rate of charge transfer will then depend on how each of these new energy levels energetically align with and couple to the donor state of the NC. By controlling ligand aggregation, in principle charge transfer rates could be selectively enhanced or suppressed.

While evidence of ligand clustering on NC surfaces has been observed in ^{1}H-NMR spectra of NC:molecule systems,[39] direct spectroscopic evidence of acceptor ligand aggregation is lacking due to the low magnitude of the transition dipole moment of commonly employed acceptor ligands. This has made it difficult to discern what role ligand aggregation plays in setting rates for NC-to-molecule exciton and charge transfer and how best to control aggregation to enhance or suppress these rates.

To address this issue, we have conducted a systematic study on a set of lead (II) sulfide (PbS) NCs functionalized with different concentrations of perylenediimide (PDI) electron acceptors to deduce how PDI aggregation on PbS surfaces impacts the rate of NC-to-molecule electron transfer. As more PDIs bind to PbS, we observe formation of mixed PDI monomer and aggregate ligand shells that increase in their degree of aggregation with PDI concentration, as evidenced by a continuous redistribution of the oscillator strength of PDI vibronic absorption bands. Photoexciting the lowest-lying exciton of PbS reveals that the average rate of PbS-to-PDI electron transfer per PDI acceptor can be reduced by nearly an order of magnitude by increasing PDI surface concentration. The reduced electron transfer rate correlates with a drop in the percentage of PDI that are monomers in the ligand shell, as inferred from fitting experimental absorption spectra to a linear combination of computed PDI monomer and aggregate lineshapes. However, the tendency for PDIs to form aggregates can be controlled by employing linkers of

varying rigidity that influence the conformational space that PDIs can explore when anchored to PbS. Using electronic structure calculations and molecular dynamics simulations, we find PDI aggregate formation slows the rate of electron transfer by reducing the ability of PDI acceptors to approach the PbS donor surface, thereby weakening PbS:PDI electronic coupling. However, while aggregation acts to suppress electron transfer in the system we examine, our calculations suggest that if the relative signs of the inter-acceptor and donor-acceptor couplings can be controlled, aggregation can instead give rise to an enhancement of charge transfer.

Our results indicate that aggregation of acceptor ligands must be considered when designing NC:molecule hybrids for applications involving photoexcited charge or exciton transfer. If controlled in a systematic way, acceptor ligand aggregation can provide a unique handle for fine-tuning rates of electron and energy transfer for a desired application.

Experimental Results

PDI ligands and PbS NCs natively passivated with oleate were synthesized using previously reported methods.[40–42] Additional synthetic details are described in the Supporting Information. We employ asymmetric PDI ligands (**Scheme 1**) that contain a swallowtail for enhanced solubility, a carboxylate group that allows attachment to a PbS NC surface, and a linker consisting of an ethyl (C2-PDI), pentyl (C5-PDI), or benzyl (Bn-PDI) group. These linkers were selected for investigation due to their differences in length and structural rigidity.

A set of oleate-passivated PbS NCs were subjected to a ligand exchange using solutions where $\langle N_{PDI} \rangle$, the mean number of PDI ligands per PbS NC, was varied from low ($\langle N_{PDI} \rangle < 1$) to high ($\langle N_{PDI} \rangle = 40$). Following each ligand exchange, PbS:PDI solutions were washed by precipitation with acetone and centrifuged. The resulting pellet was resuspended in chloroform to remove unbound oleate and PDI ligands. To determine if unbound PDI ligands remain in purified

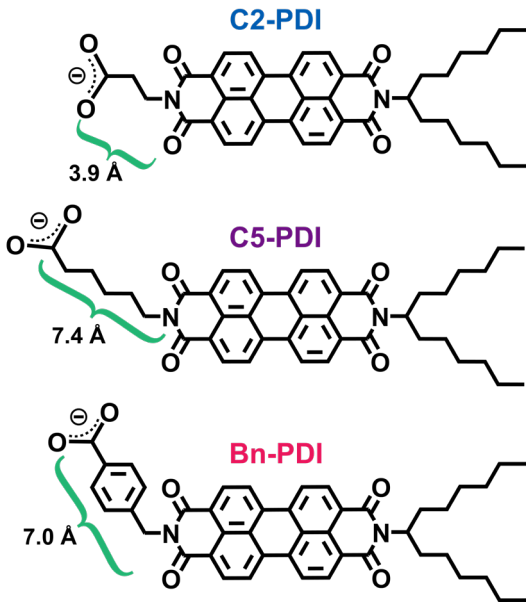

Scheme 1: Chemical structures of PDI electron-accepting ligands that attach to PbS via either an ethyl (C2-PDI), pentyl (C5-PDI), or benzyl linker (Bn-PDI). Linker lengths correspond to the carboxylate carbon to imide nitrogen distance of energy-minimized structures computed using the Universal Force Field (UFF) in Avogadro.[43]

PbS:PDI solutions, we used gel permeation chromatography to separate PDI-functionalized NCs from unbound PDI ligands (Supporting Information). No fractions were collected that contained only PDI absorption features, indicating all PDI ligands in the recovered ligand-exchanged solutions are bound to PbS.

The red trace in **Figure 2** plots the steady-state absorption spectrum of C2-PDI monomers dissolved in chloroform while corresponding spectra of C5-PDI and Bn-PDI are shown in **Figure S1** of the Supporting Information. Peak-normalized absorption spectra of each ligand are nearly indistinguishable from each other, indicating that functionalization of PDI with a linker group at the imide position has a negligible effect on the electronic structure of each ligand. This insensitivity of the absorption spectra of PDI monomers to imide substitution arises as their frontier molecular orbitals possess nodes at the imide nitrogen atoms.[44] Absorption spectra of C2-PDI, C5-PDI, and Bn-PDI monomers each exhibit a vibronic progression, peaked at its 0-0 transition at 526 nm, with peaks spaced by ~1400 cm^{-1}. This spacing corresponds to a C-C stretching mode of the

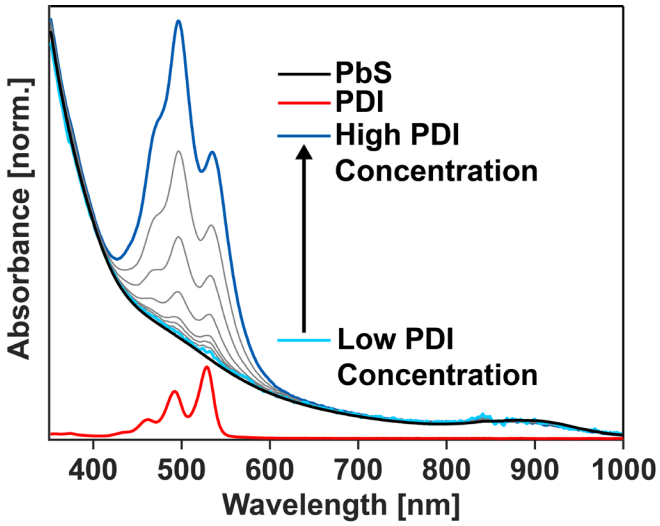

Figure 2: Steady-state absorption spectra of PbS NCs (black) and monomeric C2-PDI ligands (red) prior to ligand exchange. Post-exchange PbS:C2-PDI solutions (blue and grey) show a redistribution of the C2-PDI vibronic progression as $\langle N_{PDI} \rangle$ is varied from 0.5 – 36.9, indicating the formation of C2-PDI aggregates on the surface of PbS NCs.

perylene core and is characteristic of PDI monomers.[45–47] The appearance of this lineshape indicates that PDI ligands dissolved in solution are not aggregated prior to ligand exchange with PbS NCs.

Plotted alongside spectra of C2-PDI monomers in **Figure 2** are spectra of oleate-capped PbS NCs and the resulting PbS:C2-PDI solutions obtained following a series of ligand exchange reactions that employ differing concentrations of C2-PDI. When PDIs are exchanged onto the NC surface, we observe no change in the PbS first exciton band peaked at 880 nm. However, the spectral region wherein C2-PDI ligands absorb becomes highly modified. Notably, when C2-PDI is bound to a NC at sufficiently high concentration, we observe a redistribution of the oscillator strength of the PDI vibronic progression that favors enhanced intensity of its 0-1 and 0-2 transitions, at 490 and 460 nm respectively, over the 0-0 peak at 526 nm, and the entire absorption manifold broadens and shifts to the red by ~25 meV. Absorption spectra of PbS:C5-PDI and PbS:Bn-PDI (**Figure S2**) display similar lineshape changes as the surface concentration of PDI ligands affixed to PbS is increased. Similar changes in optical spectra of PDIs have been observed

as a result of co-facial stacking between PDI molecules[46,48–50] and indicate the formation of PDI aggregates on the surface of PbS NCs.

The observed spectral changes stem from Coulombic interactions between the dipole moments of closely-arranged PDI molecules as well as direct electron exchange interactions that originate from the spatial overlap of the frontier orbitals of co-facially stacked PDIs.[48–51] For PDI molecules affixed to a surface by tethers of the same length, we expect aggregation to lead to a side-by-side arrangement of molecules, inducing a positive sign of the Coulombic coupling and the formation of a Kasha H-aggregate.[38] Such aggregates exhibit a blue-shift of their spectral onset and a suppression of low-energy peaks in their vibronic structure in favor of higher energy transitions.[51] While we indeed observe a suppression of the 0-0 transition of each aggregate, we note that their absorption onset is shifted to slightly lower energy relative to spectra of the monomers of each PDI. This likely is the result of additional electron exchange interactions between neighboring PDIs, which if sufficiently strong can induce a spectral red-shift for an aggregate with H-type Coulombic coupling.[47,49,52] As electron exchange interactions exhibit an exponential dependence on spacing between chromophores, this red-shift suggests that neighboring PDIs affixed to a PbS surface can stack in co-facial arrangements that allow for spatial overlap of their π-systems.

To better quantify how the aggregation of PDI ligands depends on their surface concentration, we isolated their absorption spectra by subtracting features associated with PbS NCs from spectra of PbS:PDI samples (Supporting Information). **Figure 3A** shows absorption spectra of PbS:C2-PDI following removal of PbS absorption contributions. Similar background-subtracted absorption spectra for PbS:C5-PDI and PbS:Bn-PDI are shown in **Figure S3**. For all three ligands, as PDI concentration increases, optical spectra transition from monomer-like PDI

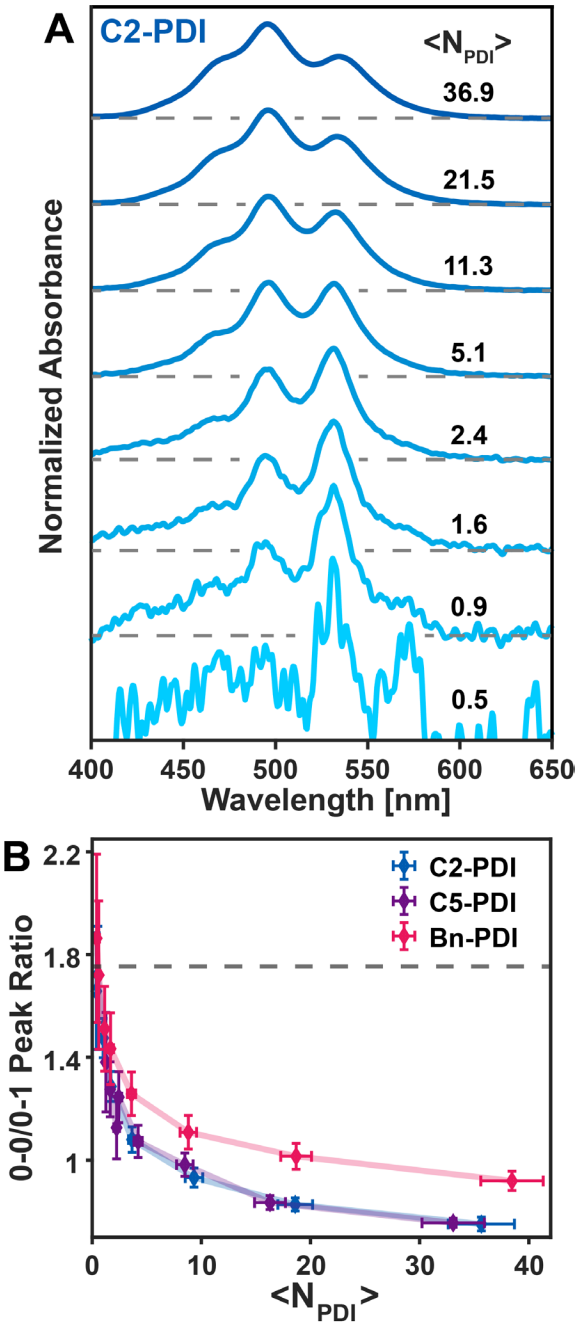

Figure 3: (A) Absorption spectra of PbS:C2-PDI following subtraction of absorption contributions from PbS NCs. Calculated values of $\langle N_{PDI} \rangle$ are listed next to each spectrum. (B) 0-0/0-1 vibronic peak height ratios as a function of $\langle N_{PDI} \rangle$. The dashed grey line indicates the average peak height ratio for PDI monomers.

features to aggregate bands, with spectra measured at intermediate PDI surface concentrations showing features of both monomers and aggregates, indicating the presence of a mixed ligand shell that contains both species.

The degree of aggregation of each PDI can be assessed by monitoring the ratio of the PDI 0-0 and 0-1 vibronic transitions as this ratio decreases as aggregation occurs. To obtain this ratio, the absorption spectra of each PDI were fit to a series of gaussians and the resulting amplitudes for the 0-0 and 0-1 vibronic peaks were compared (**Figure 3B**). Absorption spectra of C2-PDI, C5-PDI, and Bn-PDI monomers were found to exhibit nearly identical 0-0/0-1 peak ratios of 1.74, 1.77, and 1.74, respectively, which are consistent with ratios reported for other monomeric PDIs.[53] When bound to PbS in low surface concentration, all three PDI ligands show peak ratios near 1.75, the mean of the 0-0/0-1 peak ratios for all three ligands, indicating that PDIs bind as individual monomers to PbS. As the surface concentration of each PDI increases, the peak ratios display a marked decrease. For C2-PDI and C5-PDI, this ratio decreases by nearly a factor of 2 for surface concentrations as low as $\langle N_{PDI} \rangle = 5.1$, indicating significant aggregate formation. The appearance of aggregate features at such a low surface concentration is surprising given that the PbS NCs we employ contain more than 100 potential ligand binding sites.[54] This suggests that PDI aggregates arise from preferential clustering of ligands at the PbS surface. Similar behavior was reported by Green et al. who found evidence of clustered anthracene ligands at high-energy binding sites located at the corners and edges of PbS NCs.[39]

As the PDI surface concentration is increased further, the 0-0/0-1 peak ratios asymptote towards constant values, indicating the relative amounts of PDI aggregates and monomers that bind to PbS ceases to change. C2-PDI and C5-PDI asymptote towards a peak ratio of 0.7, a value that has previously been reported for PDI dimers held in a co-facial geometry via a xanthene-bridge.[53] This suggests that a significant fraction of the PDIs bound to PbS at high concentration in these systems are involved in aggregate structures. In contrast, Bn-PDI displays a limiting 0-0/0-1 peak ratio that is noticeably higher, 0.9. This indicates that at high surface concentration,

a larger fraction of Bn-PDI molecules bound to PbS remain in a monomeric state rather than form aggregates. The distinct behavior observed for Bn-PDI compared to C2-PDI and C5-PDI suggests that the chemical structure of the linking group used to attach molecules to NCs can alter their propensity to aggregate. We hypothesize that this difference in aggregation behavior stems from the higher rigidity of Bn-PDI's benzyl linker, which can act to restrict the orientational freedom required for the formation of co-facially stacked aggregates.

To examine the impact of acceptor ligand aggregation on the ability to move charge from PbS NCs to PDI electron acceptors, we employed transient absorption (TA) spectroscopy to track the photoexcited dynamics of PDI-functionalized PbS NCs. **Figure 4A** shows TA spectra of PbS NCs functionalized with a high surface concentration of C2-PDI ($\langle N_{PDI} \rangle = 33.6$) recorded following photoexcitation of PbS at 800 nm. At a delay time of 0.25 ps, a broad induced absorption appears across the visible spectrum (most clearly seen from 575 – 650 nm) that has previously been assigned to interband transitions of PbS.[40,55,56] As time advances, we observe growth of a negative band between 450 – 550 nm concomitant with strengthening of an induced absorption band peaked near 720 nm. The negative feature matches the inverse of the absorption spectrum of surface-bound C2-PDI ligands (**Figure 3A**), indicating that over time these molecules are depopulated from their ground state. The induced absorption band seen at 720 nm develops in concert with the C2-PDI ground state bleach and is consistent with prior reports of PDI radical anions ($PDI^{\bullet-}$),[57–59] indicating that photoexcitation of PbS drives the transfer of an electron to surface-bound C2-PDI molecules to produce a $PbS^{\bullet+}$:$PDI^{\bullet-}$ charge transfer state. Once formed, this state is found to persist for several hundred picoseconds before decaying to the ground state (**Figure 4B**). PbS NCs containing C5-PDI or Bn-PDI ligands exhibit similar spectral features and excited-state dynamics (**Figure S5**) as those seen for PbS:C2-PDI.

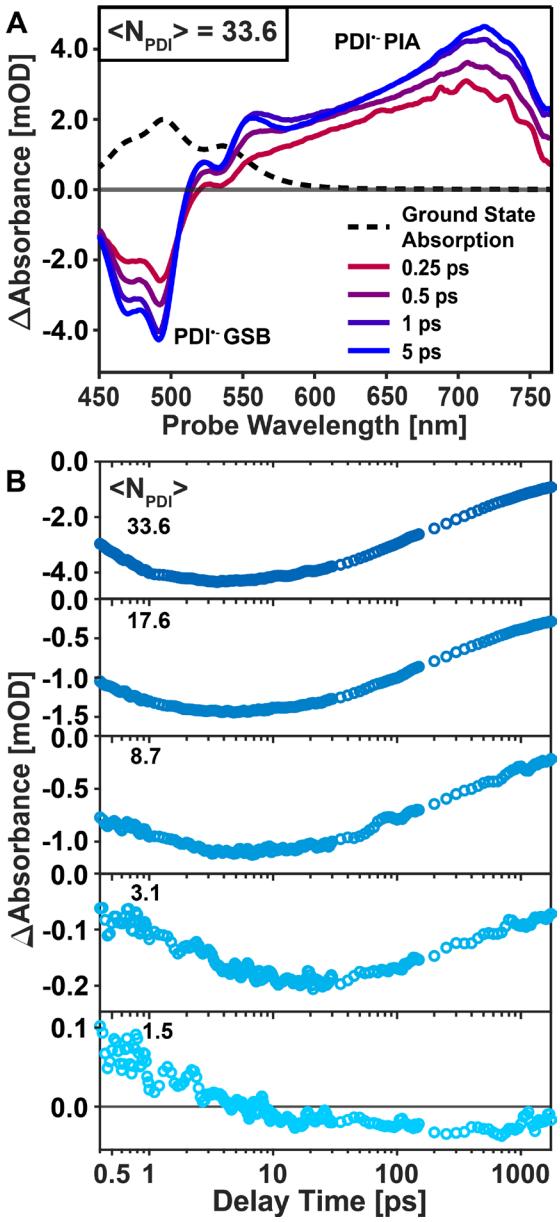

Figure 4: (A) Colored, solid traces show TA spectra of PbS:C2-PDI ($\langle N_{PDI} \rangle = 33.6$) recorded at different delay times following PbS photoexcitation at 800 nm. For comparison, the ground state absorption spectrum of C2-PDI is shown in dashed black. PIA: photoinduced absorption. GSB: ground-state bleach. (B) Kinetic traces showing the growth and decay of the integrated C2-PDI GSB as a function of $\langle N_{PDI} \rangle$.

The effect of increasing $\langle N_{PDI} \rangle$ on PbS-to-PDI electron transfer is illustrated in **Figure 4B** which tracks the C2-PDI ground-state bleach signal as a function of delay time for PbS NCs that feature different C2-PDI surface concentrations. As $\langle N_{PDI} \rangle$ increases, the signal maximum is reached at earlier delay times, indicating that the observed rate of electron transfer for the NC

ensemble, k_{ET}, increases as the surface concentration of C2-PDI increases, in accordance with our expectation from Eq. 1. Assuming all PDI molecules that bind to a surface are equally likely to accept an electron, we expect the rate of electron transfer to increase linearly with the PDI surface concentration. In practice however, Eq. 1 cannot be used to directly fit TA kinetics measured on NC ensembles as it does not account for heterogeneity in the number of PDIs that bind to different NCs in an ensemble.

To compare timescales for photoinduced electron transfer between PbS NCs that bind C2-PDI, C5-PDI, and Bn-PDI ligands, we make use of a fitting approach described by Raulerson et al.[40] that employs a kinetic model detailed by Morris-Cohen et al.[32,60] In this model, PDI ligands are taken to be dispersed among the NCs within an ensemble according to Poisson statistics. Following photoexcitation of a PbS NC, each PDI bound to its surface is assumed to be able to accept an electron with a rate, k_{ET}^0. Summing these transfer kinetics over NCs in the ensemble that bind n PDI ligands yields the following expression for the growth of the $PbS^{\bullet+}$:$PDI^{\bullet-}$ charge transfer state:

$$[PbS^{\cdot+}:PDI^{\cdot-}](t) = A * \left(1 - \sum_{n=0}^{\infty}\left(\frac{\langle N_{PDI}\rangle^n}{n!}e^{-\langle N_{PDI}\rangle}\right)\left(e^{-nk_{ET}^0 t}\right)\right), \quad (2)$$

where A is a proportionality constant. This sum can be simplified to yield the following analytic expression for the development of the charge transfer state:[32,61]

$$[PbS^{\cdot+}:PDI^{\cdot-}](t) = A * \left(1 - e^{\left(\langle N_{PDI}\rangle\left[e^{\left(-k_{ET}^0 t\right)}-1\right]\right)}\right) \quad (3)$$

Using Eq. 3, we have fit the rise of the integrated PDI ground state bleach for PbS:C2-PDI, PbS:C5-PDI, and PbS:Bn-PDI samples measured as a function of $\langle N_{PDI}\rangle$ and the resulting values of k_{ET}^0 are plotted in **Figure 5**. As $\langle N_{PDI}\rangle$ approaches zero, we expect only monomers to be bound to the surface of PbS NCs. Hence, the value of k_{ET}^0 in this limit describes how each of the linkers

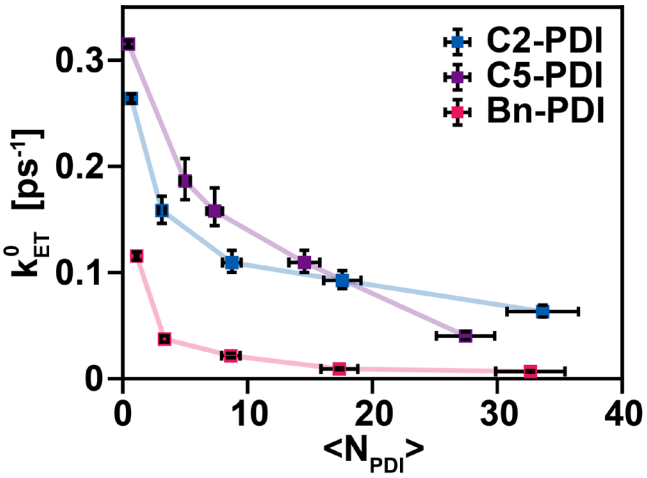

Figure 5: Average rates for photoinduced electron transfer from PbS to surface-bound PDI ligands as a function of the PDI ligand surface concentration, $\langle N_{PDI} \rangle$. The rates were extracted by applying Eq. 3 to the rise of the integrated PDI ground state bleach observed in TA spectra.

we employ impacts the rate of the electron transfer independent of effects tied to ligand aggregation. As the rate of electron transfer is expected to decrease exponentially with increasing donor:acceptor distance,[25,29] our expectation was that Bn-PDI and C5-PDI would exhibit smaller limiting values of k_{ET}^0 as compared to C2-PDI due to their linker being approximately twice as long as that of C2-PDI when fully extended. Bn-PDI indeed exhibits a limiting value of 0.12 ps^{-1} that is less than half that of C2-PDI (0.26 ps^{-1}), indicating that Bn-PDI's rigid benzyl linker restricts the ability of its PDI charge acceptor to approach the PbS surface, leading to a weakened donor-acceptor coupling relative to C2-PDI. In contrast, we find that C5-PDI exhibits a limiting rate of 0.32 ps^{-1} that is larger than that of C2-PDI, despite this ligand possessing a long alkyl linker that, when extended, is similar in length to that of Bn-PDI. This result can be rationalized if C5-PDI's alkyl linker is sufficiently flexible that it allows its PDI chromophore to bend towards the PbS surface to engage in through-space electron transfer. Data supporting this hypothesis was previously reported by Morris-Cohen and co-workers who found that increasing the length of an alkyl linker on methyl viologen ligands did not lead to a reduction in the electron transfer rate due to the ability of the charge acceptor to bend towards the NC.[60]

Examining how k_{ET}^0 changes as a function of $\langle N_{PDI} \rangle$, we find that the rate of electron transfer per PDI decreases as the PDI surface concentration of all three PDI ligands is increased. In the case of C5-PDI, this decrease is quite dramatic, as k_{ET}^0 drops by nearly an order of magnitude as $\langle N_{PDI} \rangle$ is increased from 0.5 to 27.5. In the absence of PDI ligand-ligand interactions, we would expect k_{ET}^0 to be independent of $\langle N_{PDI} \rangle$. Such behavior has been observed by Weiss and co-workers in studies that examined electron transfer from cadmium chalcogenide NCs to methyl viologen electron acceptors.[32,33] However, a key difference for the system we investigate is that we see strong spectral features that signal formation of PDI aggregates on PbS NC surfaces at high ligand loading. Our data thus suggests that aggregate formation results in a drastic slowing of photoinduced electron transfer.

Discussion

Our results reveal that we can induce acceptor ligand aggregation by increasing the concentration of acceptor ligands bound to the NC surface and that the formation of these aggregates acts to decrease k_{ET}^0. To better understand how k_{ET}^0 differs between PDI monomers and its aggregates, it is necessary to first quantify how the populations of these species within PbS ligand shells vary with PDI surface concentration. In principle, such information can be obtained by deconvoluting the absorption spectra in **Figures 3A** and **S3** into contributions from PDI monomers and aggregates if the extinction spectra for each of these species are known. While spectra of PDI monomers can be obtained from solution measurements of each PDI ligand, aggregates of these ligands are difficult to experimentally isolate. For this reason, we estimate extinction spectra of PDI aggregates using a semiempirical Holstein-type Hamiltonian model[48,51,62,63] (see Supporting Information for details). Briefly, spectra were calculated using an energy-minimized PDI structure wherein the imide side groups have been replaced with hydrogen

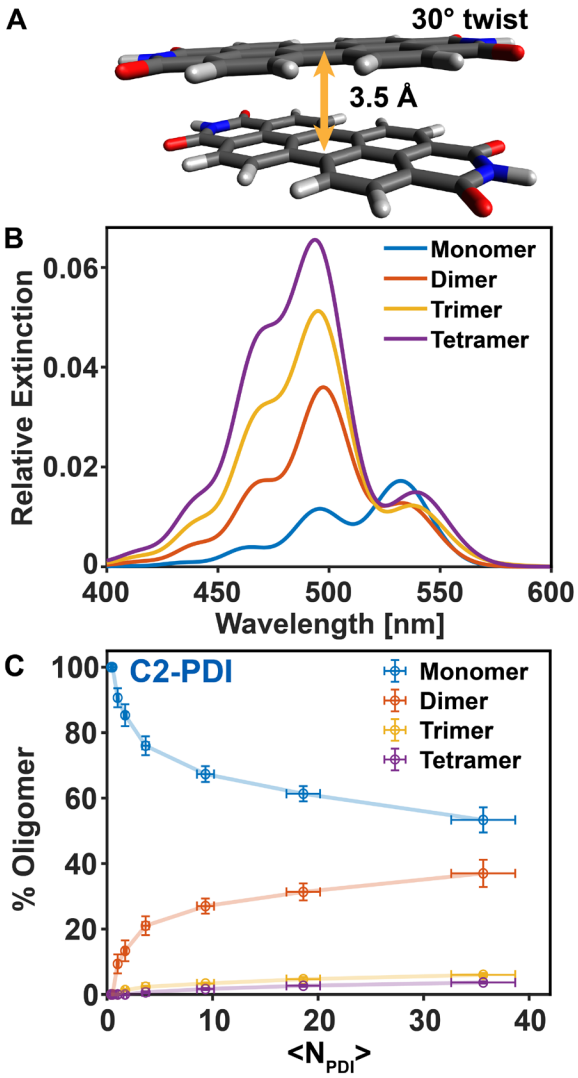

Figure 6: (A) Structure used to compute absorption spectra of PDI dimers. This structure corresponds to an energy minimum on the PDI dimer potential energy surface.[64] (B) Computed extinction spectra of PDI monomers, dimers, trimers, and tetramers used to fit absorption spectra of PDI-functionalized PbS NCs. Extinction spectra are reported on a per species basis (i.e. the dimer spectrum includes extinction contributions from both molecules that comprise the dimer, the trimer includes contributions from all three of its molecules, etc.). (C) Partitioning of monomer and aggregate species formed on the surface of PbS NCs as a function of the C2-PDI surface concentration.

atoms for computational expediency. This structure was assembled into co-facial dimer, trimer, and tetramer stacks wherein neighboring PDIs are separated by 3.5 Å and twisted by 30° about the axis normal to the plane of each PDI molecule (**Figure 6A**). This twist angle was selected as it corresponds to the global minimum of the ground-state potential energy surface for a PDI dimer.[64]

Cofacially-stacked PDIs are expected to adopt a similar orientation at PbS NC surfaces to minimize repulsive interactions between bulky swallow-tail groups on the ends of each PDI molecule, which we indeed find evidence for using molecular dynamics simulations (*vide infra*).

Calculated extinction spectra for a PDI monomer, dimer, trimer, and tetramer are shown in **Figure 6B**. Aggregate structures exhibit a suppressed 0-0 and enhanced 0-1 and 0-2 vibronic transitions, consistent with our experimental absorption spectra. To determine the fraction of monomers and aggregates that bind to the NCs, PbS-subtracted absorption spectra were fit to a linear combination of the calculated monomer and oligomer spectra where the coefficient weighting each basis spectrum defines the percentage of bound PDI molecules that constitute that species. **Figure S6** compares experimental absorption spectra for PbS:C2-PDI, PbS:C5-PDI and PbS:Bn-PDI (blue, purple, and pink traces) against the corresponding theoretical fits (black traces). We find that theoretical spectra are in good agreement with experimental absorption spectra and reproduce the ratio of 0-0 and 0-1 vibronic peak intensities highlighted in **Figure 3B**. This analysis indicates that the PbS ligand shell primarily consists of PDI monomers and dimers, with timers and tetramers contributing at most 11% to the absorption spectra at the highest PDI surface concentrations we examine (**Figures 6C** & **S7**).

For all three PDI ligands, we find the spectral contribution from monomers decreases as PDI surface concentration is increased (**Figure 7A**). As $\langle N_{PDI} \rangle$ is increased to ~30, we find C2-PDI and C5-PDI show a 45% reduction in monomer population while Bn-PDI exhibits a smaller monomer reduction on only 29%. This suggests the higher structural rigidity of Bn-PDI's benzyl linker inhibits aggregation, likely by restricting the ability of neighboring PDIs to reorient to form aggregate structures. Importantly, we find a strong correlation between changes in the percentage of PDI monomers that bind to PbS NCs and the value of k_{ET}^{0}. As the relative fraction of PDI

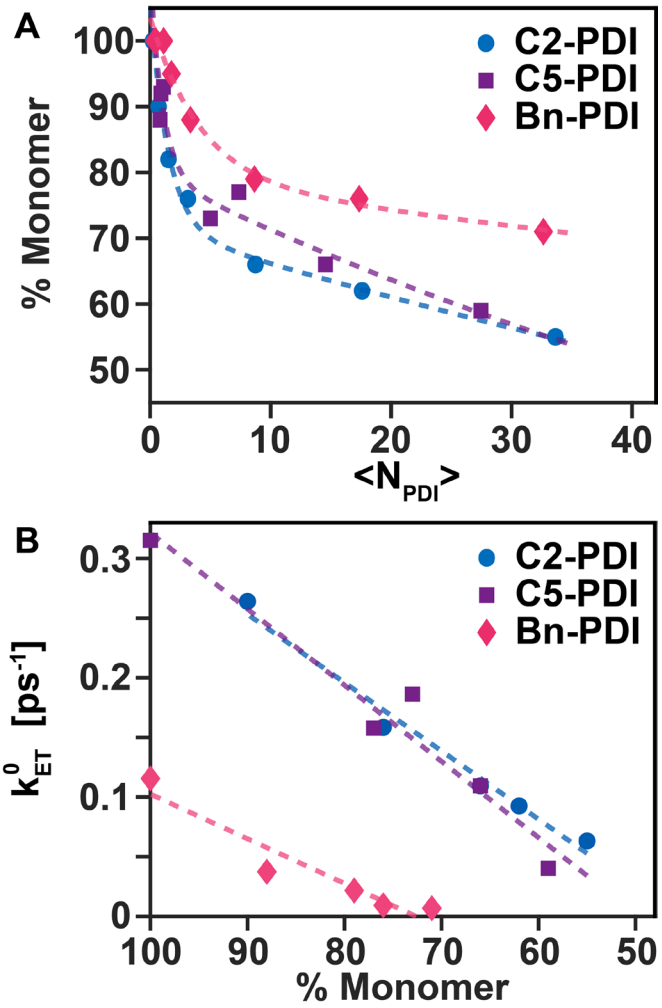

Figure 7: (A) The percentage of PDI molecules that exist as monomers when bound to PbS as a function of $\langle N_{PDI} \rangle$. The curved lines serve as guides to the eye. (B) The dependence of the average PbS-to-PDI electron transfer rate per bound PDI molecule, k_{ET}^0, as a function of the percentage of PDIs that affix to PbS as monomers. As PDI molecules in a PbS ligand shell form aggregates, k_{ET}^0 decreases. The dashed lines are linear fits that serve as guides to the eye.

monomers decreases, so too does k_{ET}^0, indicating the loss of the PDI monomer population to form aggregates is responsible for the decrease in k_{ET}^0 (**Figure 7B**).

Our results indicate that electron transfer to a PDI monomer is faster than transfer to PDI ligands that form aggregates. Several potential scenarios can possibly explain this result. First, aggregate formation could act to reduce the energetic driving force for electron transfer. As discussed in **Figure 1**, electronic coupling between charge-accepting ligand states causes them to hybridize and split in energy. Due to their energetic difference, each of these new aggregate states

will feature a different energetic driving force for electron transfer that can thus alter its rate. Second, aggregation can restrict the ability of electron acceptors to approach the PbS surface, thereby reducing their electronic coupling. Prior reports have shown that monomeric electron acceptors anchored to NCs by short alkyl chains can tilt towards the surface, thereby reducing the tunneling gap for electron transfer.[40,60] However, the formation of co-facially stacked PDI aggregates may impact how PDIs orient with respect to the PbS surface, affecting k_{ET}^{0}.

To untangle these potential structural and energetic effects, we have employed electronic structure calculations in concert with molecular dynamics simulations. We first consider the effects of electronic coupling between acceptor ligands (denoted as J) on the expected rate of electron transfer. As shown in **Figure 1**, coupling between ligands will induce their electron-accepting levels to hybridize into delocalized aggregate states. The overall rate of electron transfer can then be described by an expression akin to that derived by Taylor and Kassal[65] in which the overall rate is given by a sum of all the possible electron transfer rates from the donor to each of the aggregate levels. Unlike Ref. 65, for simplicity, we assume the outer-sphere component of the reorganization energy dominates over the inner-sphere one. Consequently, the reorganization energy is taken to be the same for charge transfer to each aggregate state. We also account for Auger-assisted electron transfer using the empirical expression of Zhu *et al.*[66]

As described in detail in the Supporting Information, the rate of electron transfer to each aggregate eigenstate depends on their energetic position relative to the PbS donor level as well as their coupling to the donor state. In the case of a PDI dimer, the individual ligand LUMO orbitals hybridize to form a symmetric and an antisymmetric level that each couple differently to a PbS NC. Assuming the electronic couplings between each of the individual PDIs within the dimer and the PbS NC are positive, the coupling of the symmetric acceptor eigenstate to the donor level will

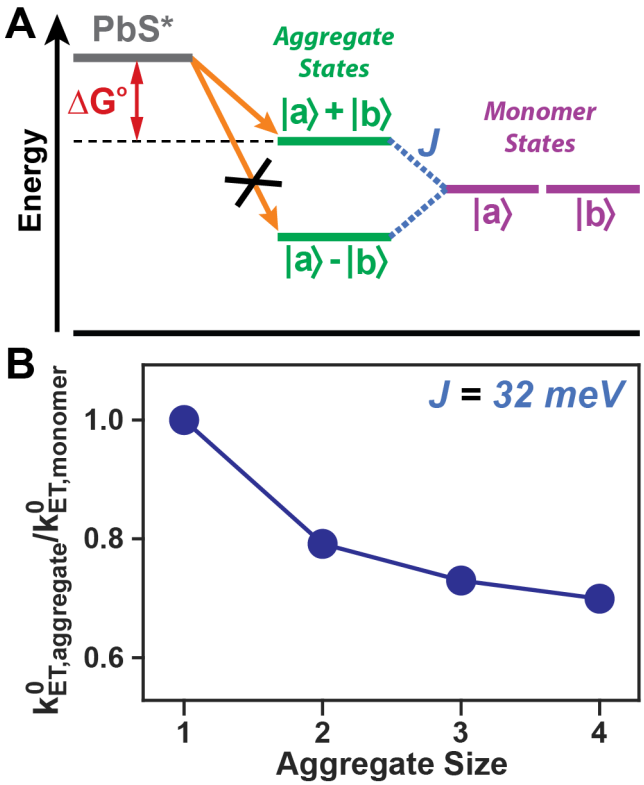

Figure 8: (A) Electronic coupling between the charge-accepting states of pairs of ligands ($|a\rangle$ and $|b\rangle$) will give rise to new states that are symmetric and asymmetric combinations of the uncoupled energy levels. Assuming the electronic coupling between the PbS donor level and each of the monomer states is the same, then only the symmetric combination of monomer levels ($|a\rangle + |b\rangle$) will be able to accept charge as the coupling between PbS and the asymmetric state ($|a\rangle - |b\rangle$) will be zero by symmetry. If the acceptor intermolecular coupling, J, is positive, then the symmetric state will be raised in energy relative to the monomer states, thereby decreasing the driving force, ΔE, for charge transfer. (B) Ratio of the computed value of k_{ET}^0 for a PDI aggregate relative to that for a PDI monomer as a function of the aggregate size. For this calculation, J was set to 32 meV on the basis of DFT calculations, the reorganization energy, λ, was set to 0.3 eV, the driving force for charge transfer to the monomer was set to -0.4 eV, and $k_B T = 26$ meV.

be enhanced (as compared to the monomer) whereas coupling of the antisymmetric level will be zero by symmetry (**Figure 8A**).[67] Consequently, electron transfer will only involve the symmetric level of the dimer. This is a situation similar to that seen in the optical absorption spectra of H- and J-type molecular dimers, wherein all of the dimers' oscillator strength is given to the symmetric state of the pair.[38,68]

In terms of electron transfer, whether the rate of transfer to the symmetric state of the dimer is enhanced or suppressed relative to that of two uncoupled monomers will depend on where this

level lies energetically with respect to the monomer level. Positive coupling between the monomer LUMOs will raise the energy of the symmetric PDI dimer state relative to that of PDI monomers. This will act to lower the driving force for electron transfer, and consequently its rate. In contrast, negative coupling between PDI LUMOs will lower the dimer state energy, increasing both the driving force for charge transfer and its rate. Therefore, of particular importance here is the sign of the PDI-PDI (acceptor-acceptor) coupling (relative to the PbS-PDI donor-acceptor coupling), which sets the energetic position of the symmetric level of the dimer relative to that of a PDI monomer.

To estimate the sign and magnitude of the acceptor-acceptor coupling, we performed DFT calculations on a C2-PDI dimer bound to a PbS NC. For this calculation, we considered a prototypical lead-rich $Pb_{55}S_{38}$ NC[69] coordinated with 32 formate ligands and a C2-PDI dimer whose hexyl side chains have been truncated to methyl groups for computational expediency. To make the DFT calculations tractable, this NC possesses a diameter of ~1.6 nm, which is smaller than the 3 nm diameter NCs we investigate experimentally. Similarly, for computational expediency, oleate ligands used to solubilize NCs experimentally have been replaced with isoelectronic formate ligands. We expect these choices to have minimal impact on the magnitude of the acceptor-acceptor coupling as this quantity is largely set by intermolecular interactions between neighboring PDI molecules rather than their association with the PbS NC and its oleate ligand shell. Following a geometry optimization, we evaluated the acceptor-acceptor coupling as half of the energy splitting between the lowest unoccupied orbitals of the C2-PDI ligands. Using the PBE0-D3 functional,[70,71] 6-31G* basis set on the light atoms, and lanl2dz basis set with the corresponding effective core potentials on Pb and S in NWChem,[72] we find $|J| = 32$ meV. We take this value to be positive, as well as the PbS-PDI donor-acceptor couplings, as this would lead to a

suppression of the PbS-to-PDI electron transfer rate (see Supporting Information for details). To compute the electron transfer rate for PDI trimers, tetramers, and larger aggregates, we consider ideal 1D stacks of PDIs wherein the nearest-neighbor coupling adopts the value we compute for a dimer.

Figure 8B plots the average electron transfer rate for PDI aggregates, k_{ET}^{0}, relative to the electron transfer rate for a PDI monomer as a function of the aggregate size. We find the positive intermolecular coupling computed between PDI molecules indeed leads to a lessening of the average electron transfer rate as the size of the PDI aggregate increases. While this general trend is consistent with our experiments, we find the predicted drop in electron transfer rate with increasing aggregate size is modest relative to our experimental observations. Specifically, our calculations in **Figure 8B** predict that a C2-PDI dimer should only exhibit a 20% slowdown in its rate of electron transfer relative to a pair of PDI monomers. However, our experimental data in **Figure 7A** shows that a PbS NC whose C2-PDI ligand shell is composed of only 24% aggregates exhibits a 40% reduction in k_{ET}^{0}, which is twice that predicted by our calculation for a ligand shell composed exclusively of dimers. This disagreement becomes even more apparent as a NC's aggregate surface coverage increases as we experimentally observed a 76% reduction in k_{ET}^{0} for NCs whose ligand shells are made up of only 55% aggregates. Moreover, we note that electron transfer to the asymmetric level of a PDI dimer is symmetry-forbidden only if the two acceptors are coupled to the PbS donor state with equal strengths – a condition likely to be partially violated in real systems due to structural heterogeneity in how neighboring PDIs affix themselves to the PbS surface. In addition, the intermolecular coupling between neighboring PDIs is known to change rapidly as one PDI slips along another, making it possible for structural fluctuations of a dimer to transiently alter the magnitude and sign of the PDI acceptor-acceptor coupling, further

mitigating the predicted rate decrease when applying this formalism to a real system. Taken in total, these discrepancies mean that electronic effects tied to the formation of aggregate states alone are insufficient to explain the decrease we observe in k_{ET}^{0} with increasing PDI surface concentration.

To explore if PDI dimerization impacts k_{ET}^{0} by restricting how these ligands orient with respect to a PbS surface, we have employed molecular dynamics (MD) methods. All MD simulations are performed using GROMACS[73] and are described in detail in the Supporting Information. Briefly, we make use of an OPLS-based force field[74,75] and use standard OPLS parameters for organic matter. A combination of parameters taken from Fan et al.[76] and Heinz et al.[77] are used to describe organic-PbS interactions, with the former being used for carboxylate-lead interactions while the latter is used for any remaining non-covalent interactions. Standard OPLS partial charges are used, supplemented by ESP-derived partial charges for PbS, carboxylate, and PDI atoms.

We again considered a non-stoichiometric $Pb_{55}S_{38}$ NC coordinated with 34 deprotonated ligands, either thirty-three oleate and one C2-PDI ligand or thirty-two oleate and two C2-PDI ligands, solvated in chloroform. In contrast to our DFT calculations, we have included here the bulky oleate ligands used experimentally as they can be expected to play an important role in determining the possible C2-PDI geometries on the surface of the NC. Interactions between the NC and ligands are captured solely through non-bonding electrostatic and Lennard-Jones potentials, which allowed for the diffusion of ligands on the surface of the NC. When two C2-PDI ligands were included in the simulation, they were initially placed co-facially and in close vicinity of each other to facilitate dimer formation. To enhance the phase-space sampling, we carried out cyclical simulated annealing on the two considered systems. For each, we performed a 10 ns

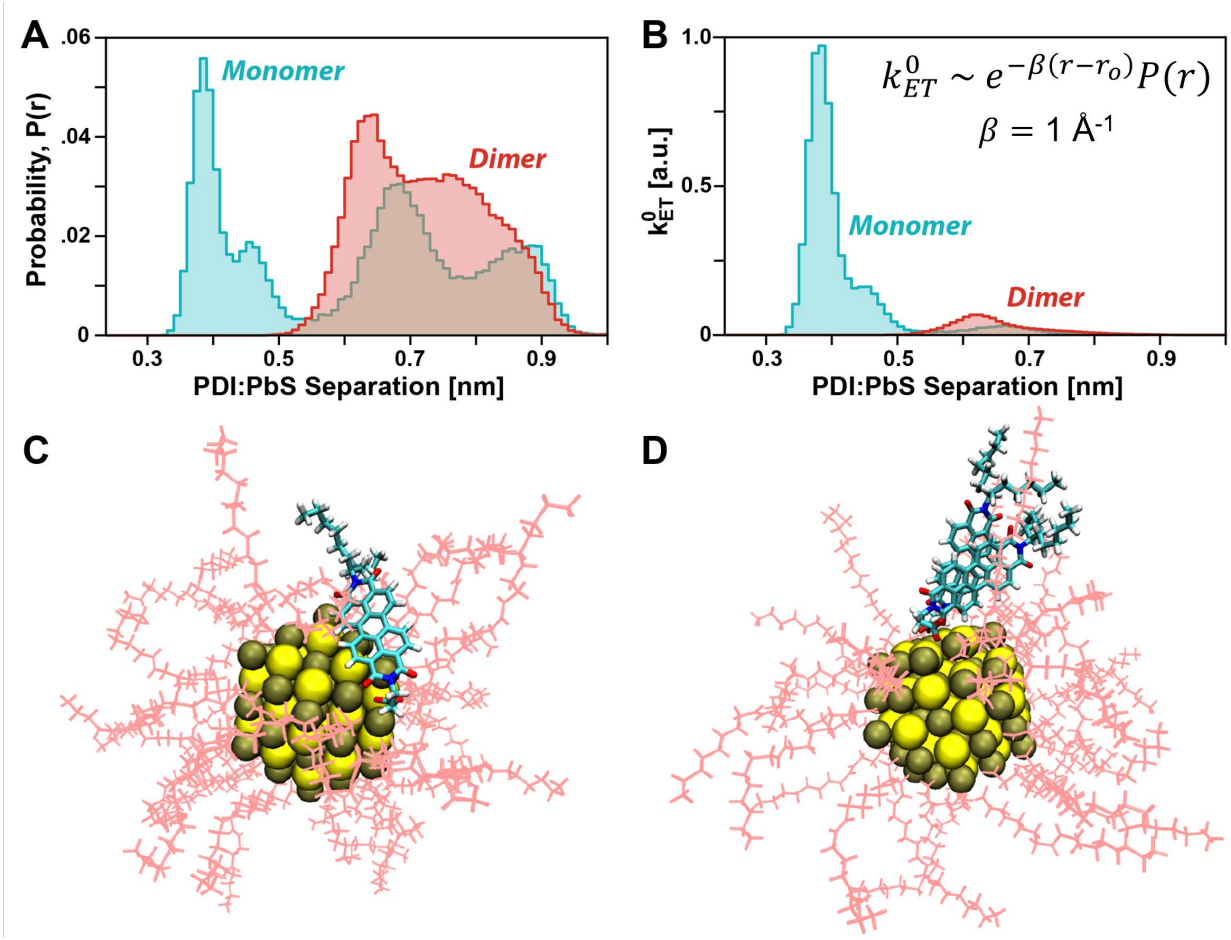

Figure 9: (A) Distributions of the PDI center-to-PbS surface distance over the course of the simulations. The distribution shown for the dimer represents behavior exhibited by the individual PDIs within the dimer pair. (B) Product of the distributions shown in panel (A) and a decaying exponential, $exp[-\beta(r - r_0)]$ with β set to 1 Å^{-1} and r_o to 3.2 Å in both cases. (C, D) Representative geometries adopted by the monomer (C) and dimer (D) PDI ligands. S atoms are shown in yellow, Pb atoms in brown, oleate chains in pink. The corresponding PDI center-to-PbS surface distances are 3.8 Å for the monomer in (C) and 6.4 and 7.9 Å for the dimer in (D).

annealing cycle followed by a 100 ns production run. This simulated annealing procedure was repeated ten times, resulting in 1 μs of simulation time for the monomer and dimer systems (see Supporting Information for details).

Figure 9A plots the distribution of distances between the center of the C2-PDI ligands (taken as the mean of the C2-PDI nitrogen positions) and the PbS surface for simulation runs involving a C2-PDI monomer and dimer. We find the short carbon chain of C2-PDI monomers is sufficiently flexible that it allows these ligands to explore a large distribution of conformations on

the PbS surface, similar to how an inflatable tube man, or air puppet, contorts and swings its body into different bent geometries when in contact with the wind. Importantly, we find that these ligands spend ~1/3 of their time in geometries wherein they partially lay down on the NC surface (**Figure 9C**). Such geometries are expected to promote charge transfer from PbS to C2-PDI monomers. In contrast, we find van der Waals interactions between C2-PDI dimers are such that these molecules prefer to associate with one another rather than with the PbS surface. Consequently, dimers are generally found to adopt geometries wherein their cores are situated far from the PbS surface to facilitate co-facial stacking of the molecules within the dimer (**Figure 9D**).

The different orientations adopted by PDI monomers and dimers about the PbS surface leads to differences in their donor-acceptor couplings. Co-facial stacking of C2-PDI dimers prohibits them from adopting geometries that result in very large donor-acceptor coupling while C2-PDI monomers can readily explore geometries wherein the donor-acceptor coupling is large. As the donor-acceptor coupling is predicted to decrease exponentially with increasing PbS-PDI separation,[6] in **Figure 9B** we attempt to predict how the geometry distributions plotted in **Figure 9A** will each contribute to PbS-to-PDI electron transfer by weighting these distributions by an exponential function, $exp[-\beta(r - r_0)]$, where β is the decay constant and r_0 is the closest-contact distance, which is set to 3.2 Å for both distributions as this is the smallest PDI:PbS surface separation observed in the simulations. For β, we consider a value of 1 Å^{-1}, which is consistent with our prior work investigating electron transfer from PbS to C2-PDI ligands[40] as well as prior reports of electron transfer from NCs to surface-bound ligands.[11,78] We find that due to this exponential distance scaling, close contact geometries formed by C2-PDI monomers carry a disproportionate contribution to the overall electron transfer rate. We find that when all structures adopted by monomers and dimers in our simulation runs are averaged over, the rate of electron

transfer exhibited by C2-PDI monomers is 7× faster than that of C2-PDI dimers. We note that subtle increases in β lead to predictions that more strongly favor the contributions of C2-PDI monomers over dimers to electron transfer. For example, doubling β yields a 70× faster rate of electron transfer for C2-PDI monomers over dimers. These observations suggest van der Waals interactions that give rise to PDI aggregation also act to slow the rate of PbS-to-PDI electron transfer by restricting the range of motion of PDI ligands and their ability to approach the PbS surface.

Conclusions

We have investigated the impact of acceptor aggregation on the dynamics of photoinduced charge transfer from NCs to surface-bound electron acceptors. By using a system comprised of PbS NCs interfaced with PDI electron acceptors that show large spectroscopic changes upon PDI aggregation, we can quantify the onset of PDI aggregation with changing surface concentration. Using ultrafast TA spectroscopy, we find as aggregation occurs, the average rate of electron transfer per acceptor from photoexcited PbS NCs to surface-bound PDI molecules decreases. Using a combination of electronic structure calculations and MD simulations, we ascribe this slowdown to the formation of PDI dimers on the surface of PbS NCs. While PDI monomers can explore a range of geometries when bound to PbS, van der Waals interactions between members of a PDI dimer pair restrict their ability to adopt geometries that favor strong coupling to PbS, lowering the rate at which they accept charge.

Interestingly, we find the effects of aggregation can be mitigated to some degree by altering the chemical structure of the linkages used to anchor electron acceptors to PbS. Employing short, flexible linkers may be ideal for the design of future NC:molecule systems as they can allow acceptors to approach the NC surface when acceptors are bound at low surface concentrations. At

high concentration, these short, flexible linkers can also aid in maintaining a short donor-acceptor distance even when the acceptors may tilt away from the NC surface due to aggregation. While we observe that aggregation hinders electron transfer in the system we investigate, we note that if the sign of the intermolecular coupling between neighboring surface ligands can be controlled, acceptor aggregation offers a potential pathway for enhancing electron transfer rates by tuning the free energy for this process.

Overall, our results highlight that acceptor ligand aggregation can be used to enhance or suppress the migration of charge between NCs and molecular acceptors. As such, the aggregation of acceptor ligands provides researchers with a new handle for designing functional materials that shuttle charge or energy across hybrid NC:molecule interfaces.

Supporting Information Available

Synthetic details for the preparation of C2-PDI, C5-PDI, and Bn-PDI ligands, oleate-passivated PbS NCs and PbS:PDI ligand exchange solutions; Steady-state and transient absorption measurements; Removal of PbS contributions to steady-state absorption spectra; Calculation of $\langle N_{PDI} \rangle$ from steady-state absorption spectra of PDI-functionalized PbS NCs; Calculation of integrated 0-0/0-1 vibronic peak ratios; Kinetic model used to determine k_{ET}^{0} from TA spectra; Holstein Hamiltonian model used compute absorption spectra of PDI oligomers; Quantification of PDI aggregates bound to PbS NCs; Computational methods used for electronic structure calculations and MD simulations as well as additional MD results.

Author Information

Corresponding Authors

Sean T. Roberts; OCRID ID: 0000-0002-3322-3687; Email: roberts@cm.utexas.edu

Peter J. Rossky; OCRID ID: 0000-0002-0461-4179; Email: peter.rossky@rice.edu

Authors

Danielle M. Cadena; OCRID ID: 0000-0002-8121-0223

Jakub K. Sowa; OCRID ID: 0000-0003-4104-2664

Christopher D. Wight; OCRID ID: 0000-0003-3389-1762

Daniel E. Cotton; OCRID ID: 0000-0002-5170-7108

Cole Hoffman; ORCID ID: 0000-0003-0328-5729

Holden Wagner; ORCID ID: 0000-0001-8718-6474

Jessica T. Boette; ORCID ID: 0000-0002-3838-5925

Emily K. Raulerson; OCRID ID: 0000-0002-3145-5644

Brent L. Iverson; OCRID ID: 0000-0001-7974-3605

Acknowledgements

This work was supported by the Center for Adapting Flaws into Features, an NSF Center for Chemical Innovation supported by grant CHE-2124983, and the Welch Foundation via grants F-1885 and F-1188. DMC thanks the National Science Foundation for support from the Graduate Research Fellowship Program under grant DGE-1610403. We would like to further thank the UT NMR facility for the Bruker AVIII HD 500 (NIH Grant 1 S10 OD021508-01). This work was supported in part by the Big-Data Private-Cloud Research Cyberinfrastructure MRI-award funded by the NSF under grant CNS-1338099 and by Rice University's Center for Research Computing (CRC). JKS and PJR gratefully acknowledge High Performance Computing (HPC) resources and support provided to Rice University by Advanced Micro Devices (AMD).

References

(1) Brett, M. W.; Gordon, C. K.; Hardy, J.; Davis, N. J. L. K. The Rise and Future of Discrete Organic–Inorganic Hybrid Nanomaterials. *ACS Phys. Chem. Au* **2022**, *2* (5), 364–387.

(2) Garakyaraghi, S.; Castellano, F. N. Nanocrystals for Triplet Sensitization: Molecular Behavior from Quantum-Confined Materials. *Inorg. Chem.* **2018**, *57* (5), 2351–2359.

(3) Huang, Z.; Tang, M. L. Semiconductor Nanocrystal Light Absorbers for Photon Upconversion. *J. Phys. Chem. Lett.* **2018**, 6198–6206.

(4) Lu, H.; Huang, Z.; Martinez, M. S.; Johnson, J. C.; Luther, J. M.; Beard, M. C. Transforming Energy Using Quantum Dots. *Energy Environ. Sci.* **2020**, *13* (5), 1347–1376.

(5) Jiang, Y.; Weiss, E. A. Colloidal Quantum Dots as Photocatalysts for Triplet Excited State Reactions of Organic Molecules. *J. Am. Chem. Soc.* **2020**, *142* (36), 15219–15229.

(6) Zhu, H.; Yang, Y.; Wu, K.; Lian, T. Charge Transfer Dynamics from Photoexcited Semiconductor Quantum Dots. *Annu. Rev. Phys. Chem.* **2016**, *67* (1), 259–281.

(7) Han, Y.; He, S.; Wu, K. Molecular Triplet Sensitization and Photon Upconversion Using Colloidal Semiconductor Nanocrystals. *ACS Energy Lett.* **2021**, *6* (9), 3151–3166.

(8) Scholes, G. D. Controlling the Optical Properties of Inorganic Nanoparticles. *Adv. Funct. Mater.* **2008**, *18* (8), 1157–1172.

(9) Kroupa, D. M.; Arias, D. H.; Blackburn, J. L.; Carroll, G. M.; Granger, D. B.; Anthony, J. E.; Beard, M. C.; Johnson, J. C. Control of Energy Flow Dynamics between Tetracene Ligands and PbS Quantum Dots by Size Tuning and Ligand Coverage. *Nano Lett.* **2018**, *18* (2), 865–873.

(10) Gray, V.; Allardice, J. R.; Zhang, Z.; Dowland, S.; Xiao, J.; Petty, A. J.; Anthony, J. E.; Greenham, N. C.; Rao, A. Direct vs Delayed Triplet Energy Transfer from Organic Semiconductors to Quantum Dots and Implications for Luminescent Harvesting of Triplet Excitons. *ACS Nano* **2020**, *14* (4), 4224–4234.

(11) Tagliazucchi, M.; Tice, D. B.; Sweeney, C. M.; Morris-Cohen, A. J.; Weiss, E. A. Ligand-Controlled Rates of Photoinduced Electron Transfer in Hybrid CdSe Nanocrystal/Poly(Viologen) Films. *ACS Nano* **2011**, *5* (12), 9907–9917.

(12) Kamat, P. V. Manipulation of Charge Transfer Across Semiconductor Interface. A Criterion That Cannot Be Ignored in Photocatalyst Design. *J. Phys. Chem. Lett.* **2012**, *3* (5), 663–672.

(13) Weiss, E. A. Designing the Surfaces of Semiconductor Quantum Dots for Colloidal Photocatalysis. *ACS Energy Lett.* **2017**, *2* (5), 1005–1013.

(14) Nienhaus, L.; Wu, M.; Geva, N.; Shepherd, J. J.; Wilson, M. W. B.; Bulović, V.; Van Voorhis, T.; Baldo, M. A.; Bawendi, M. G. Speed Limit for Triplet-Exciton Transfer in Solid-State PbS Nanocrystal-Sensitized Photon Upconversion. *ACS Nano* **2017**, *11* (8), 7848–7857.

(15) Huang, Z.; Li, X.; Mahboub, M.; Hanson, K. M.; Nichols, V. M.; Le, H.; Tang, M. L.; Bardeen, C. J. Hybrid Molecule–Nanocrystal Photon Upconversion Across the Visible and Near-Infrared. *Nano Lett.* **2015**, *15* (8), 5552–5557.

(16) Mongin, C.; Garakyaraghi, S.; Razgoniaeva, N.; Zamkov, M.; Castellano, F. N. Direct Observation of Triplet Energy Transfer from Semiconductor Nanocrystals. *Science* **2016**, *351*, 369–372.

(17) Jiang, Y.; Wang, C.; Rogers, C. R.; Kodaimati, M. S.; Weiss, E. A. Regio- and Diastereoselective Intermolecular [2+2] Cycloadditions Photocatalysed by Quantum Dots. *Nat. Chem.* **2019**, *11* (11), 1034–1040.

(18) Singh-Rachford, T. N.; Castellano, F. N. Triplet Sensitized Red-to-Blue Photon Upconversion. *J. Phys. Chem. Lett.* **2010**, *1* (1), 195–200.

(19) Yanai, N.; Kimizuka, N. New Triplet Sensitization Routes for Photon Upconversion: Thermally Activated Delayed Fluorescence Molecules, Inorganic Nanocrystals, and Singlet-to-Triplet Absorption. *Acc. Chem. Res.* **2017**, *50* (10), 2487–2495.

(20) Zhou, J.; Liu, Q.; Feng, W.; Sun, Y.; Li, F. Upconversion Luminescent Materials: Advances and Applications. *Chem. Rev.* **2015**, *115* (1), 395–465.

(21) Wu, M.; Congreve, D. N.; Wilson, M. W. B.; Jean, J.; Geva, N.; Welborn, M.; Van Voorhis, T.; Bulović, V.; Bawendi, M. G.; Baldo, M. A. Solid-State Infrared-to-Visible Upconversion Sensitized by Colloidal Nanocrystals. *Nat. Photonics* **2015**, *10* (1), 31–34.

(22) Mahboub, M.; Huang, Z.; Tang, M. L. Efficient Infrared-to-Visible Upconversion with Subsolar Irradiance. *Nano Lett.* **2016**, *16* (11), 7169–7175.

(23) Tripathi, N.; Ando, M.; Akai, T.; Kamada, K. Efficient NIR-to-Visible Upconversion of Surface-Modified PbS Quantum Dots for Photovoltaic Devices. *ACS Appl. Nano Mater.* **2021**, *4* (9), 9680–9688.

(24) Imperiale, C. J.; Green, P. B.; Hasham, M.; Wilson, M. W. B. Ultra-Small PbS Nanocrystals as Sensitizers for Red-to-Blue Triplet-Fusion Upconversion. *Chem. Sci.* **2021**, *12* (42), 14111–14120.

(25) Wang, H.; McNellis, E. R.; Kinge, S.; Bonn, M.; Cánovas, E. Tuning Electron Transfer Rates through Molecular Bridges in Quantum Dot Sensitized Oxides. *Nano Lett.* **2013**, *13* (11), 5311–5315.

(26) Xu, Z.; Huang, Z.; Li, C.; Huang, T.; Evangelista, F. A.; Tang, M. L.; Lian, T. Tuning the Quantum Dot (QD)/Mediator Interface for Optimal Efficiency of QD-Sensitized Near-Infrared-to-Visible Photon Upconversion Systems. *ACS Appl. Mater. Interfaces* **2020**, *12* (32), 36558–36567.

(27) Li, X.; Huang, Z.; Zavala, R.; Tang, M. L. Distance-Dependent Triplet Energy Transfer between CdSe Nanocrystals and Surface Bound Anthracene. *J. Phys. Chem. Lett.* **2016**, *7* (11), 1955–1959.

(28) Huang, Z.; Xu, Z.; Huang, T.; Gray, V.; Moth-Poulsen, K.; Lian, T.; Tang, M. L. Evolution from Tunneling to Hopping Mediated Triplet Energy Transfer from Quantum Dots to Molecules. *J. Am. Chem. Soc.* **2020**, *142* (41), 17581–17588.

(29) Xu, Z.; Cotlet, M. Quantum Dot–Bridge–Fullerene Heterodimers with Controlled Photoinduced Electron Transfer. *Angew. Chem. Int. Ed.* **2011**, *50* (27), 6079–6083.

(30) Morris-Cohen, A. J.; Malicki, M.; Peterson, M. D.; Slavin, J. W. J.; Weiss, E. A. Chemical, Structural, and Quantitative Analysis of the Ligand Shells of Colloidal Quantum Dots. *Chem. Mater.* **2013**, *25* (8), 1155–1165.

(31) Dexter, D. L. A Theory of Sensitized Luminescence in Solids. *J. Chem. Phys.* **1953**, *21* (5), 836–850.

(32) Morris-Cohen, A. J.; Frederick, M. T.; Cass, L. C.; Weiss, E. A. Simultaneous Determination of the Adsorption Constant and the Photoinduced Electron Transfer Rate for a CdS Quantum Dot–Viologen Complex. *J. Am. Chem. Soc.* **2011**, *133* (26), 10146–10154.

(33) Leng, H.; Loy, J.; Amin, V.; Weiss, E. A.; Pelton, M. Electron Transfer from Single Semiconductor Nanocrystals to Individual Acceptor Molecules. *ACS Energy Lett.* **2016**, *1* (1), 9–15.

(34) Zhang, J.; Kouno, H.; Yanai, N.; Eguchi, D.; Nakagawa, T.; Kimizuka, N.; Teranishi, T.; Sakamoto, M. Number of Surface-Attached Acceptors on a Quantum Dot Impacts Energy Transfer and Photon Upconversion Efficiencies. *ACS Photonics* **2020**, *7* (7), 1876–1884.

(35) Boulesbaa, A.; Issac, A.; Stockwell, D.; Huang, Z.; Huang, J.; Guo, J.; Lian, T. Ultrafast Charge Separation at CdS Quantum Dot/Rhodamine B Molecule Interface. *J. Am. Chem. Soc.* **2007**, *129* (49), 15132–15133.

(36) Huang, Z.; Simpson, D. E.; Mahboub, M.; Li, X.; Tang, M. L. Ligand Enhanced Upconversion of Near-Infrared Photons with Nanocrystal Light Absorbers. *Chem. Sci.* **2016**, *7* (7), 4101–4104.

(37) Marcus, R. A. On the Theory of Electrochemical and Chemical Electron Transfer Processes. *Can. J. Chem.* **1959**, *37* (1), 155–163.

(38) Kasha, M.; Rawls, H. R.; El-Bayoumi, M. A. The Exciton Model in Molecular Spectroscopy. *Pure Appl. Chem.* **1965**, *11*, 371–392.

(39) Green, P. B.; Yarur Villanueva, F.; Imperiale, C. J.; Hasham, M.; Demmans, K. Z.; Burns, D. C.; Wilson, M. W. B. Directed Ligand Exchange on the Surface of PbS Nanocrystals: Implications for Incoherent Photon Conversion. *ACS Appl. Nano Mater.* **2021**, *4* (6), 5655–5664.

(40) Raulerson, E. K.; Cadena, D. M.; Jabed, M. A.; Wight, C. D.; Lee, I.; Wagner, H. R.; Brewster, J. T.; Iverson, B. L.; Kilina, S.; Roberts, S. T. Using Spectator Ligands to Enhance Nanocrystal-to-Molecule Electron Transfer. *J. Phys. Chem. Lett.* **2022**, 1416–1423.

(41) Holman, M. W.; Liu, R.; Adams, D. M. Single-Molecule Spectroscopy of Interfacial Electron Transfer. *J. Am. Chem. Soc.* **2003**, *125* (41), 12649–12654.

(42) Kessler, M. L.; Starr, H. E.; Knauf, R. R.; Rountree, K. J.; Dempsey, J. L. Exchange Equilibria of Carboxylate-Terminated Ligands at PbS Nanocrystal Surfaces. *Phys. Chem. Chem. Phys.* **2018**, *20* (36), 23649–23655.

(43) Hanwell, M. D.; Curtis, D. E.; Lonie, D. C.; Vandermeersch, T.; Zurek, E.; Hutchison, G. R. Avogadro: An Advanced Semantic Chemical Editor, Visualization, and Analysis Platform. *J. Cheminformatics* **2012**, *4*, 1–17.

(44) Wurthner, F. Perylene Bisimide Dyes as Versatile Building Blocks for Functional Supramolecular Architectures. *Chem Commun* **2004**, *0*, 1564–1579.

(45) Huang, C.; Barlow, S.; Marder, S. R. Perylene-3,4,9,10-Tetracarboxylic Acid Diimides: Synthesis, Physical Properties, and Use in Organic Electronics. *J. Org. Chem.* **2011**, *76* (8), 2386–2407.

(46) Giaimo, J. M.; Lockard, J. V.; Sinks, L. E.; Scott, A. M.; Wilson, T. M.; Wasielewski, M. R. Excited Singlet States of Covalently Bound, Cofacial Dimers and Trimers of Perylene-3,4:9,10-Bis(Dicarboximide)s. *J. Phys. Chem. A* **2008**, *112* (11), 2322–2330.

(47) Le, A. K.; Bender, J. A.; Arias, D. H.; Cotton, D. E.; Johnson, J. C.; Roberts, S. T. Singlet Fission Involves an Interplay between Energetic Driving Force and Electronic Coupling in Perylenediimide Films. *J. Am. Chem. Soc.* **2018**, *140* (2), 814–826.

(48) Oleson, A.; Zhu, T.; Dunn, I. S.; Bialas, D.; Bai, Y.; Zhang, W.; Dai, M.; Reichman, D. R.; Tempelaar, R.; Huang, L.; Spano, F. C. Perylene Diimide-Based Hj- and HJ-Aggregates: The Prospect of Exciton Band Shape Engineering in Organic Materials. *J. Phys. Chem. C* **2019**, *123* (33), 20567–20578.

(49) Hestand, N. J.; Spano, F. C. Interference between Coulombic and CT-Mediated Couplings in Molecular Aggregates: H- to J-Aggregate Transformation in Perylene-Based π-Stacks. *J. Chem. Phys.* **2015**, *143* (24), 244707.

(50) Kazmaier, P. M.; Hoffmann, R. A Theoretical Study of Crystallochromy. Quantum Interference Effects in the Spectra of Perylene Pigments. *J. Am. Chem. Soc.* **1994**, *116* (21), 9684–9691.

(51) Hestand, N. J.; Spano, F. C. Molecular Aggregate Photophysics beyond the Kasha Model: Novel Design Principles for Organic Materials. *Acc. Chem. Res.* **2017**, *50* (2), 341–350.

(52) Gisslén, L.; Scholz, R. Crystallochromy of Perylene Pigments: Interference between Frenkel Excitons and Charge-Transfer States. *Phys. Rev. B* **2009**, *80* (11), 115309.

(53) Brown, K. E.; Salamant, W. A.; Shoer, L. E.; Young, R. M.; Wasielewski, M. R. Direct Observation of Ultrafast Excimer Formation in Covalent Perylenediimide Dimers Using Near-Infrared Transient Absorption Spectroscopy. *J. Phys. Chem. Lett.* **2014**, *5* (15), 2588–2593.

(54) Kessler, M. L.; Dempsey, J. L. Mapping the Topology of PbS Nanocrystals through Displacement Isotherms of Surface-Bound Metal Oleate Complexes. *Chem. Mater.* **2020**, *32* (6), 2561–2571.

(55) Bender, J. A.; Raulerson, E. K.; Li, X.; Goldzak, T.; Xia, P.; Van Voorhis, T.; Tang, M. L.; Roberts, S. T. Surface States Mediate Triplet Energy Transfer in Nanocrystal–Acene Composite Systems. *J. Am. Chem. Soc.* **2018**, *140* (24), 7543–7553.

(56) Cho, B.; Peters, W. K.; Hill, R. J.; Courtney, T. L.; Jonas, D. M. Bulklike Hot Carrier Dynamics in Lead Sulfide Quantum Dots. *Nano Lett.* **2010**, *10* (7), 2498–2505.

(57) Zeman, C. J.; Kim, S.; Zhang, F.; Schanze, K. S. Direct Observation of the Reduction of Aryl Halides by a Photoexcited Perylene Diimide Radical Anion. *J. Am. Chem. Soc.* **2020**, *142* (5), 2204–2207.

(58) Ahrens, M. J.; Kelley, R. F.; Dance, Z. E. X.; Wasielewski, M. R. Photoinduced Charge Separation in Self-Assembled Cofacial Pentamers of Zinc-5,10,15,20-Tetrakis(Perylenediimide)Porphyrin. *Phys. Chem. Chem. Phys.* **2007**, *9* (12), 1469.

(59) Supur, M.; Fukuzumi, S. Photodriven Electron Transport within the Columnar Perylenediimide Nanostructures Self-Assembled with Sulfonated Porphyrins in Water. *J. Phys. Chem. C* **2012**, *116* (44), 23274–23282.

(60) Morris-Cohen, A. J.; Peterson, M. D.; Frederick, M. T.; Kamm, J. M.; Weiss, E. A. Evidence for a Through-Space Pathway for Electron Transfer from Quantum Dots to Carboxylate-Functionalized Viologens. *J. Phys. Chem. Lett.* **2012**, *3* (19), 2840–2844.

(61) Utterback, J. K.; Wilker, M. B.; Brown, K. A.; King, P. W.; Eaves, J. D.; Dukovic, G. Competition between Electron Transfer, Trapping, and Recombination in CdS Nanorod–Hydrogenase Complexes. *Phys. Chem. Chem. Phys.* **2015**, *17* (8), 5538–5542.

(62) Yamagata, H.; Maxwell, D. S.; Fan, J.; Kittilstved, K. R.; Briseno, A. L.; Barnes, M. D.; Spano, F. C. HJ-Aggregate Behavior of Crystalline 7,8,15,16-Tetraazaterrylene: Introducing a New Design Paradigm for Organic Materials. *J. Phys. Chem. C* **2014**, *118* (49), 28842–28854.

(63) Cotton, D. E.; Moon, A. P.; Roberts, S. T. Using Electronic Sum-Frequency Generation to Analyze the Interfacial Structure of Singlet Fission-Capable Perylenediimide Thin Films. *J. Phys. Chem. C* **2020**, *124* (21), 11401–11413.

(64) Engel, E.; Leo, K.; Hoffmann, M. Ultrafast Relaxation and Exciton–Exciton Annihilation in PTCDA Thin Films at High Excitation Densities. *Chem. Phys.* **2006**, *325* (1), 170–177.

(65) Taylor, N. B.; Kassal, I. Generalised Marcus Theory for Multi-Molecular Delocalised Charge Transfer. *Chem. Sci.* **2018**, *9* (11), 2942–2951.

(66) Zhu, H.; Yang, Y.; Hyeon-Deuk, K.; Califano, M.; Song, N.; Wang, Y.; Zhang, W.; Prezhdo, O. V.; Lian, T. Auger-Assisted Electron Transfer from Photoexcited Semiconductor Quantum Dots. *Nano Lett.* **2014**, *14* (3), 1263–1269.

(67) As explained in detail in the Supporting Information, only the relative signs of the PDI-PDI and PDI-PbS electronic couplings are relevant to determining if electron transfer will be enhanced or suppressed to the symmetric and asymmetric aggregate states. It is possible to redefine any of the particular coupling constants provided this is done in a consistent manner.

(68) Knoester, J. Optical Properties of Molecular Aggregates. In *Proceedings of the International School of Physics "Enrico Fermi" Course CXLIX*; Agranovich, M., La Rocca, G. C., Eds.; IOS Press: Amsterdam, 2002; pp 149–186.

(69) Kim, D.; Kim, D.-H.; Lee, J.-H.; Grossman, J. C. Impact of Stoichiometry on the Electronic Structure of PbS Quantum Dots. *Phys Rev Lett* **2013**, *110* (19), 196802.

(70) Grimme, S.; Antony, J.; Ehrlich, S.; Krieg, H. A Consistent and Accurate *Ab Initio* Parametrization of Density Functional Dispersion Correction (DFT-D) for the 94 Elements H-Pu. *J. Chem. Phys.* **2010**, *132* (15), 154104.

(71) Adamo, C.; Barone, V. Toward Reliable Density Functional Methods without Adjustable Parameters: The PBE0 Model. *J. Chem. Phys.* **1999**, *110* (13), 6158–6170.

(72) Valiev, M.; Bylaska, E. J.; Govind, N.; Kowalski, K.; Straatsma, T. P.; Dam, H. J. J. V.; Wang, D.; Nieplocha, J.; Apra, E.; Windus, T. L.; Jong, W. A. de. NWChem: A Comprehensive and Scalable Open-Source Solution for Large Scale Molecular Simulations. *Comput. Phys. Commun.* **2010**, *181* (9), 1477–1489.

(73) Abraham, M. J.; Murtola, T.; Schulz, R.; Páll, S.; Smith, J. C.; Hess, B.; Lindahl, E. GROMACS: High Performance Molecular Simulations through Multi-Level Parallelism from Laptops to Supercomputers. *SoftwareX* **2015**, *1–2*, 19–25.

(74) Jorgensen, W. L.; Maxwell, D. S.; Tirado-Rives, J. Development and Testing of the OPLS All-Atom Force Field on Conformational Energetics and Properties of Organic Liquids. *J. Am. Chem. Soc.* **1996**, *118* (45), 11225–11236.

(75) Dodda, L. S.; Cabeza de Vaca, I.; Tirado-Rives, J.; Jorgensen, W. L. LigParGen Web Server: An Automatic OPLS-AA Parameter Generator for Organic Ligands. *Nucleic Acids Res.* **2017**, *45* (W1), W331–W336.

(76) Fan, Z.; Koster, R. S.; Wang, S.; Fang, C.; Yalcin, A. O.; Tichelaar, F. D.; Zandbergen, H. W.; van Huis, M. A.; Vlugt, T. J. H. A Transferable Force Field for CdS-CdSe-PbS-PbSe Solid Systems. *J. Chem. Phys.* **2014**, *141* (24), 244503.

(77) Heinz, H.; Lin, T.-J.; Kishore Mishra, R.; Emami, F. S. Thermodynamically Consistent Force Fields for the Assembly of Inorganic, Organic, and Biological Nanostructures: The INTERFACE Force Field. *Langmuir* **2013**, *29* (6), 1754–1765.

(78) Wang, H.; McNellis, E. R.; Kinge, S.; Bonn, M.; Cánovas, E. Tuning Electron Transfer Rates through Molecular Bridges in Quantum Dot Sensitized Oxides. *Nano Lett.* **2013**, *13* (11), 5311–5315.

Table of Contents Graphic: